NASA TECHNICAL NOTE

NASA TN D-3645

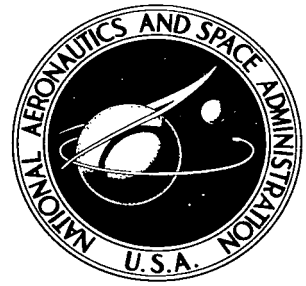

NASA TN D-3645

COMPARISON OF ONE- AND TWO-DIMENSIONAL HEAT-TRANSFER CALCULATIONS IN CENTRAL FIN-TUBE RADIATORS

by Norbert O. Stockman, Edward C. Bittner, and Earl L. Sprague

Lewis Research Center
Cleveland, Ohio

NATIONAL AERONAUTICS AND SPACE ADMINISTRATION • WASHINGTON, D. C. • SEPTEMBER 1966

NASA TN D-3645

COMPARISON OF ONE- AND TWO-DIMENSIONAL HEAT-TRANSFER CALCULATIONS IN CENTRAL FIN-TUBE RADIATORS

By Norbert O. Stockman, Edward C. Bittner, and Earl L. Sprague

Lewis Research Center
Cleveland, Ohio

NATIONAL AERONAUTICS AND SPACE ADMINISTRATION

For sale by the Clearinghouse for Federal Scientific and Technical Information
Springfield, Virginia 22151 – Price $2.00

COMPARISON OF ONE- AND TWO-DIMENSIONAL HEAT-TRANSFER CALCULATIONS IN CENTRAL FIN-TUBE RADIATORS

by Norbert O. Stockman, Edward C. Bittner, and Earl L. Sprague

Lewis Research Center

SUMMARY

An analysis is given of the two-dimensional heat transfer, including gray body radiant interchange, in the cross section of a central fin-tube radiator panel. Results of this analysis are used to evaluate several one-dimensional methods of varying complexity for calculating the heat rejection rate of a central fin-tube radiator panel. Most methods gave good agreement with the two-dimensional results. In view of the excellent agreement of one of the simpler methods which neglects tube wall temperature drop and accounts for radiant interchange between fin and tube simply by using the projected area of the tube, it seems unwarranted to use the more complex methods which gave no better agreement. Details of the numerical method of solution of the two-dimensional equations are given in an appendix.

INTRODUCTION

Electric power generation systems for space applications must reject large amounts of waste heat. At the present state of the art, the most likely method of rejecting this heat is by means of a radiator that utilizes some sort of fin and tube configuration. Various fin and tube combinations have been proposed, but only the central fin-tube geometry (fig. 1) will be considered in this report. Since the radiator represents a large portion of the powerplant weight, it must be accurately designed. Radiator design calculations are usually based on the assumption of one-dimensional heat transfer in the cross section of the fin and tube panel. Several different methods have been used to compute the heat rejection from central fin-tube panels (e.g., refs. 1 to 8). These methods contain varying degrees of complexity, and it is not obvious which methods are more accurate.

In order to evaluate the one-dimensional methods, two-dimensional calculations of fin-tube heat transfer were carried out at NASA Lewis Research Center. These calcula-

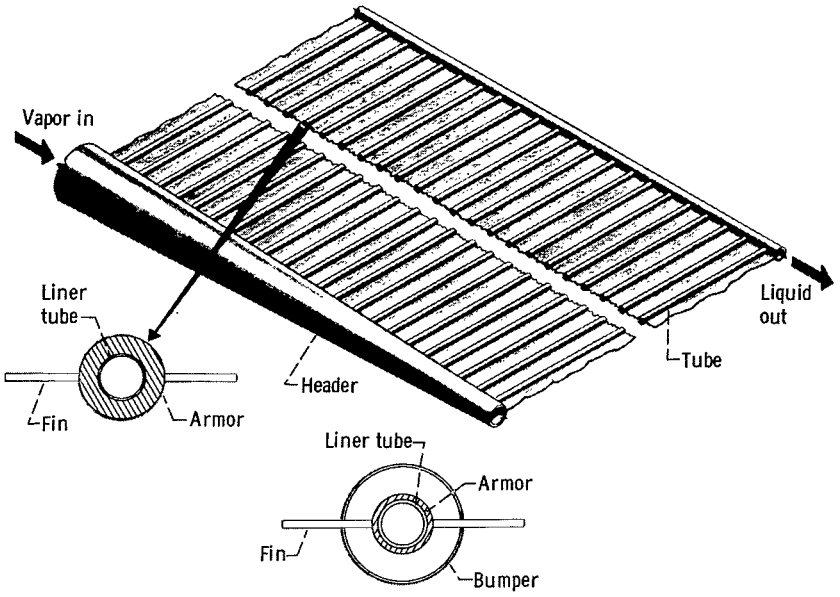

Figure 1. - Fin-tube radiator.

tions involved fewer assumptions than any of the one-dimensional methods and therefore are assumed to give a more accurate representation of the heat rejection. The analysis of the two-dimensional conduction in the cross section of a central fin-tube radiator panel with radiation from both surfaces and radiant interchange among the fin and tube surfaces is presented herein. The numerical method of solution is detailed in an appendix. Heat rejection obtained by the two-dimensional calculations is compared to that obtained by several different one-dimensional methods for 39 specific design geometries divided into the following three groups: (1) 13 miscellaneous designs for various power system applications; (2) 11 cases arbitrarily created to study the effect of changes in the fin-tube design variables on the comparison between one- and two-dimensional results; and (3) 15 off-design configurations based on a near-minimum-weight design for a Brayton cycle radiator.

ANALYSIS

The heat rejection rate of the cross section of the fin-tube panel of a radiator of the type shown in figure 1 will be computed by several different methods. Details of the two-dimensional analysis, including the calculation of the heat rejection rate, will be given, and formulas for calculating the heat rejection rate by several one-dimensional methods will be presented without detailed development.

Assumptions

All the methods (one- and two-dimensional) are based on steady-state heat conduction in the cross section of the fin and tube, radiation from both fin and tube surfaces, and the following specific assumptions (other more restrictive assumptions are required for calculating heat rejection rate by the various one-dimensional methods, and these will be given later with the formulas for heat rejection rate for each method):

(1) The radiator is infinitely long and made up of an infinite number of identical finned tubes.

(2) The inside tube wall is isothermal both longitudinally and circumferentially.

(3) The tubes and fins are made of the same material, and the material properties are assumed invariant with temperature.

(4) If there is a liner (as in fig. 1), it is of the same material as the tube and is in perfect thermal contact with the tube.

(5) Incident radiation from external sources such as Sun and planets and adjacent vehicle components is accounted for by a completely encompassing surface of constant temperature called the equivalent sink temperature T_s (ref. 9). This temperature is assumed to be the same on both sides of the radiator.

(6) Radiating surfaces are gray at a prescribed value of emittance invariant with temperature.

(7) Absorptance is equal to emittance and equal to one minus the reflectance.

The assumptions of the same sink temperature on both sides of the radiator and the same inside temperature for all tubes assures symmetry about the three center lines of the section as shown in figure 2, and thus only the shaded portion need be analyzed. Radiant interchange with surfaces outside the shaded region is included, however. It should also be pointed out that, in the two-dimensional analysis, the outside tube surface is not isothermal, and radiant interchange between individual points (increments of area) on the fin and tube surfaces is taken into account. Furthermore, this interchange extends into the axial direction (perpendicular to the plane of the cross section) and is accounted for in the development of the interchange view factor (see next section).

Since the one-dimensional methods require all the assumptions of the two-dimensional

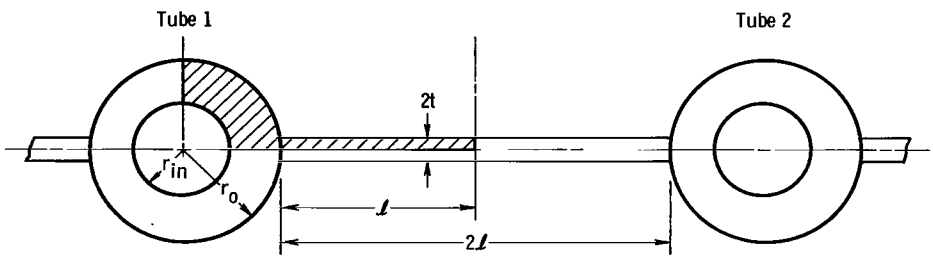

Figure 2. - Two-dimensional cross section of fin-tube radiator showing region analyzed (shaded area).

plus additional ones, the two-dimensional results are the limit to which the one-dimensional results tend with increasing refinement. Thus the two-dimensional heat rejection is used as the standard to evaluate the relative merits of the one-dimensional methods. In the next section, the differential equation and boundary conditions governing the two-dimensional heat transfer in the fin cross section under the assumptions listed previously will be presented.

Equations and Boundary Conditions

The steady-state two-dimensional heat flow in the fin and tube cross section is given by

$$\nabla^2 T = 0 \tag{1}$$

where T is the temperature. (All symbols are defined in appendix A.) The Laplacian operator ∇^2 is written in polar coordinates in the tube and in rectangular coordinates in the fin (fig. 3) to simplify grid generation for the numerical solution.

Thus, in the tube

$$\frac{1}{r}\frac{\partial T}{\partial r} + \frac{\partial^2 T}{\partial r^2} + \frac{1}{r^2}\frac{\partial^2 T}{\partial \varphi^2} = 0 \tag{2}$$

and in the fin

$$\frac{\partial^2 T}{\partial x^2} + \frac{\partial^2 T}{\partial y^2} = 0 \tag{3}$$

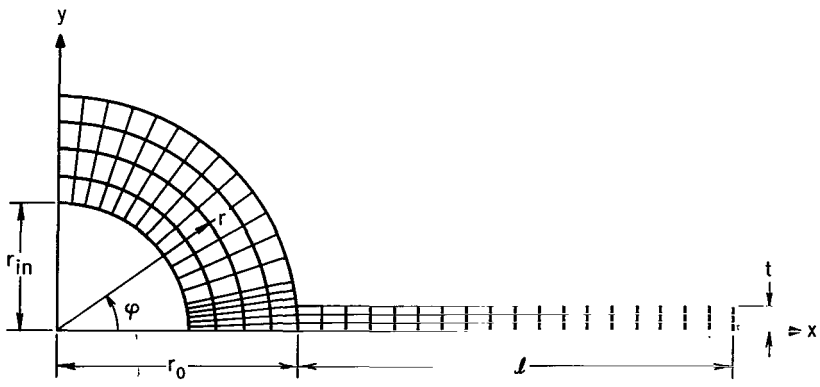

Figure 3. - Sample grid for numerical solution.

These are the two partial differential equations which must be solved. The solutions must also satisfy the following boundary conditions. Along the inside tube wall at $r = r_{in}$, the temperature is prescribed:

$$T(r_{in}, \varphi) = T_{in} \tag{4}$$

There is no heat flow across the lines $\varphi = 0$ and $\varphi = (\pi/2)$ in the tube because of symmetry, so

$$\left(\frac{\partial T}{\partial \varphi}\right)_{\varphi=0} = \left(\frac{\partial T}{\partial \varphi}\right)_{\varphi=(\pi/2)} = 0 \tag{5}$$

Also, because of symmetry, there is no heat flow across the lines $y = 0$ and $x = \ell + r_o$ in the fin, so that

$$\left(\frac{\partial T}{\partial y}\right)_{y=0} = \left(\frac{\partial T}{\partial x}\right)_{x=\ell+r_o} = 0 \tag{6}$$

On the surface of the tube at $r = r_o$ there is radiation to space where the sink temperature is T_s and interchange with surfaces of the fin and the adjacent tube. The boundary condition for net heat rejection from the tube surface can be written as

$$-k\left(\frac{\partial T}{\partial r}\right)_{r=r_o} = \epsilon \sigma T^4 - \alpha H = \epsilon (\sigma T^4 - H) \tag{7a}$$

where ϵ is the emittance, α is the absorptance of the surface, and H is the incident radiation including that from the sink and from other parts of the raditor surface. Similarly on the surface of the fin at $y = t$, the net heat rejection is

$$-k \frac{\partial T}{\partial y} = \epsilon (\sigma T^4 - H) \tag{7b}$$

Since that part of the incident radiation H contributed by the radiator surface is unknown and must be determined as part of the solution of the problem, H must be written in a form in which the radiator surface radiation appears explicitly. The equation for H, derived in appendix B, is

$$H_{dA^*} = \int_A B_{dA}\, dF_{dA^*\text{-}dA} + \sigma T_s^4 \left(1 - \int_A dF_{dA^*\text{-}dA}\right) \tag{8}$$

where B_{dA} is the radiosity (the total energy per unit time and unit area) leaving an element dA on the fin-tube surface and for a particular element dA^* is given by

$$B_{dA^*} = \epsilon \sigma T_{dA^*}^4 + \rho H_{dA^*} \tag{9}$$

Substituting equation (8) into equation (9) and replacing ρ by $1 - \epsilon$ yield

$$B_{dA^*} = \epsilon \sigma T_{dA^*}^4 + (1 - \epsilon)\left[\int_A B_{dA}\, dF_{dA^*\text{-}dA} + \sigma T_s^4 \left(1 - \int_A dF_{dA^*\text{-}dA}\right)\right] \tag{10}$$

In equations (8) to (10) $dF_{dA^*\text{-}dA}$ is the view factor from a particular element dA^* to any other element dA; that is, it is that fraction of the total heat per unit time leaving dA^* which strikes dA. The integrals in these equations represent integrals over all parts of the fin and tube visible from dA^*. Thus, for example, if dA^* is on the left tube (fig. 4), then

$$\int_A dF_{dA^*\text{-}dA} = \int_{x_L}^{x_U} dF_{r_o d\varphi_1\text{-}dx} + \int_{\varphi_{2L}}^{\varphi_{2U}} dF_{r_o d\varphi_1\text{-}r_o d\varphi_2} \tag{11}$$

where $dF_{r_o d\varphi_1\text{-}dx}$ is the view factor from the element $r_o\, d\varphi_1$ on tube 1 to the element dx on the fin, x_L and x_U are the lower and upper limits, respectively, of visibility on the fin from $r_o\, d\varphi_1$, $dF_{r_o d\varphi_1\text{-}r_o d\varphi_2}$ is the view factor from element $r_o\, d\varphi_1$ on tube 1

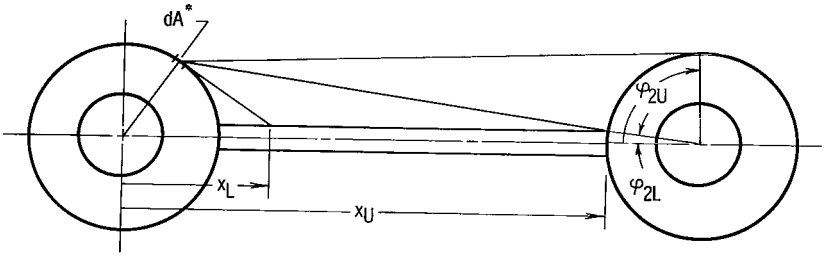

Figure 4. - Example of limits of visibility.

to element $r_o\, d\varphi_2$ on tube 2, and φ_{2L} and φ_{2U} are the lower and upper limits, respectively, of visibility on tube 2 from $r_o\, d\varphi_1$. (View factors and limits of visibility for several fin-tube radiator configurations are given in ref. 10.)

It should be noted that the areas here (and heat rejection rates later) are per unit axial length. This is to avoid infinite quantities since the axial length is assumed infinite. The view factors, however, are actually between elements of area of infinite length. (This presents no problem since view factors are fractional quantities and may be defined for infinite areas.) For example, the view factor $dF_{r_o d\varphi_1 - dx}$ is that portion of the radiation leaving the area $r_o\, d\varphi_1$ by infinite length on tube 1 and striking the area dx by infinite length on the fin. It can be seen that the radiation leaving the surface at a certain axial location on the tube but striking a different axial location on the fin is accounted for in the view factor.

Equations (2) to (8) and equation (10) in addition to the prescribed geometry r_{in}, r_o, ℓ, and t and the temperatures T_{in} and T_s determine the temperature distribution throughout the fin and tube. Equations (2) and (3) are differential equations in T; equation (10) is an integral equation in B; and T and B are related through equations (7) and (8). The equations were solved numerically on an IBM 7094 using a finite difference block overrelaxation method. Details of the numerical method of solution are given in appendix C.

Heat Rejection

The temperature distribution resulting from the solution of the equations of the preceding section is used to obtain a net heat rejection rate. The net heat rejection rate is also calculated by several one-dimensional methods for comparison with the two-dimensional results.

Two-dimensional. - Once the two-dimensional temperature distribution has been obtained, the net heat rejected Q_{2D} by the radiator per unit axial length for one quadrant can be obtained by integrating the left-hand side of equation (7a) over the tube outer surface and the left-hand side of equation (7b) over the fin outer surface; that is,

$$Q_{2D} = \int_{\varphi=\sin^{-1}(t/r_o)}^{\varphi=(\pi/2)} - k \frac{\partial T}{\partial r}\, r_o\, d\varphi + \int_{x=\sqrt{r_o^2-t^2}}^{x=r_o+\ell} - k \frac{\partial T}{\partial y}\, dx \qquad (12)$$

One-dimensional. - Several one-dimensional methods of calculating the net heat rejection rate will be considered. The formula and a brief description of each method,

which will hereinafter be referred to by its number, follows. All methods are based on the assumptions of constant tube outer surface temperature and of one-dimensional heat conduction in a radiating fin. The conduction in the fin is accounted for by a fin efficiency or an overall efficiency. The fin efficiency depends, in general, on two dimensionless parameters: the conductance parameter $\lambda = \epsilon\sigma T_b^3 \ell^2/kt$, and the sink temperature ratio T_s/T_b. The temperature T_b is the fin base temperature and is equal to T_o or T_{in} depending on whether or not the tube wall temperature drop is taken into account. When radiant interchange with the tube is taken into account, an overall efficiency is used that depends on λ and T_s/T_b and also on a third parameter, the fin-tube profile ratio ℓ/r_o.

The items that differ from method to method are whether or not a radial one-dimensional temperature drop across the tube is considered (i. e., whether T_b equals T_o or T_{in}); how radiant interchange between the radiator surfaces is accounted for, if at all; what area is used for the tube radiating surface; and how nonblackbody effects (ϵ) are handled. In all methods except (6), the nonblackbody effect is handled simply by introducing ϵ into the formula for Q. The methods, which follow, are summarized in table I.

Method 1:

$$Q_1 = \epsilon\sigma\left(T_{in}^4 - T_s^4\right)\left(\eta_{in}\ell + \frac{\pi}{2} r_o\right) \tag{13}$$

where η_{in} is the fin efficiency based on a fin base temperature equal to T_{in}. Fin efficiency for this and the next three methods includes the effect of the sink temperature T_s but not the effect of interchange with the adjacent tubes.

No temperature drop in the tube is considered (i. e., $T_b = T_{in}$), radiant interchange is neglected, and the actual area of the tube is used. The fin efficiency η_{in} is a function primarily of λ_{in} and secondarily of T_s/T_{in} and can be obtained from reference 9.

Method 2:

$$Q_2 = \epsilon\sigma\left(T_{in}^4 - T_s^4\right)\left(\eta_{in}\ell + r_o\right) \tag{14}$$

This is the same as method 1 except that the tube projected area is used instead of the actual area.

TABLE I. - SUMMARY OF ONE-DIMENSIONAL METHODS OF CALCULATING HEAT REJECTION RATE Q

Method	Formula	Temperature drop across tube wall	Interchange	Tube area
1	$Q_1 = \epsilon\sigma\left(T_{in}^4 - T_s^4\right)\left(\eta_{in}\ell + \frac{\pi}{2} r_o\right)$	No	None	Actual
2	$Q_2 = \epsilon\sigma\left(T_{in}^4 - T_s^4\right)(\eta_{in}\ell + r_o)$	No	None	Projected
3	$Q_3 = \epsilon\sigma\left(T_o^4 - T_s^4\right)(\eta_o\ell + r_o)$	Yes	None	Projected
4	$Q_4 = 0.85\ \epsilon\sigma\left(T_o^4 - T_s^4\right)\left(\eta_o\ell + \frac{\pi}{2} r_o\right)$	Yes	Approximated by factor of 0.85	Actual
5	$Q_5 = \eta_T\epsilon\sigma\left(T_o^4 - T_s^4\right)(\ell + r_o)$	Yes	Accounted for in η_T based on λ_o	Projected
6	$Q_6 = \eta_r^*\epsilon\sigma\left(T_o^4 - T_s^4\right)(\ell + r_o)$	Yes	Accounted for in η_r^* based on N_c	Projected

Method 3:

$$Q_3 = \epsilon\sigma\left(T_o^4 - T_s^4\right)(\eta_o\ell + r_o) \tag{15}$$

This is the same as method 2 except that a temperature drop across the tube wall is considered and the fin efficiency η is based on fin base temperature equal to the tube outside wall temperature and is a function of λ_o and T_s/T_o.

Method 4:

$$Q_4 = 0.85\epsilon\sigma\left(T_o^4 - T_s^4\right)\left(\eta_o\ell + \frac{\pi}{2} r_o\right) \tag{16}$$

This method uses the tube wall temperature drop and the actual area of the tube and accounts for the radiant interchange by the approximate interchange factor of 0.85. The results of reference 8 are based on this method.

Method 5:

$$Q_5 = \eta_T\epsilon\sigma\left(T_o^4 - T_s^4\right)(\ell + r_o) \tag{17}$$

This method uses the temperature drop in the tube and the projected area of the tube. Both the radiant interchange and the fin temperature distribution are accounted for by an overall effectiveness η_T which is a function of λ_o, T_s/T_o, and ℓ/r_o (see, e.g., refs. 4 and 6).

Method 6:

$$Q_6 = \eta_r^* \bar{\epsilon} \sigma \left(T_o^4 - T_s^4\right) (\ell + r_o) \tag{18}$$

This method is similar to method 5 except that η_r^* is for a blackbody and is based on N_c instead of λ_o, where $N_c = \lambda_o/\epsilon$, and the nonblackbody effect is accounted for by an aparent emissivity $\bar{\epsilon}$. The apparent emissivity accounts for the multiple reflections among the fin and tube surfaces by considering the fin and tubes to be an isothermal cavity of specified local surface emittance ϵ. The apparent emissivity is a function of ϵ (held constant in this report), ℓ/r_o, and T_s/T_o, while η_r^* is a function of N_c, ℓ/r_o, and T_s/T_o. This method is developed in reference 5.

Overall Radiator Efficiency

The heat rejection rates calculated by both the one-dimensional and two-dimensional analyses are normalized by dividing by an "ideal" heat rejection rate Q_{id} to form a so-called radiator or heat rejection efficiency; thus,

$$\eta = \frac{Q}{Q_{id}} \tag{19}$$

The advantage of comparing all the analyses on the basis of η is that the resulting values always lie between 0 and 1 (except method 1 in one case) regardless of the size or temperature level of the radiator section. The normalizing factor was arbitrarily chosen as

$$Q_{id} = \epsilon \sigma \left(T_{in}^4 - T_s^4\right) (\ell + r_o) \tag{20}$$

that is, the ideal heat rejection rate is based on the inside wall temperature and the projected area of the tube.

An additional advantage for the use of Q_{id} is that the efficiency for the one-dimensional analyses can be expressed in terms of nondimensional parameters, and

these same parameters can be carried over to the two-dimensional analysis.

Two-dimensional. - To facilitate comparison of one- and two-dimensional methods, the two-dimensional equations are nondimensionalized in appendix D in such a way that the usual one-dimensional parameters appear. It is shown that the two-dimensional heat transfer depends on λ_{in}, ℓ/r_o, θ_s (which are one-dimensional parameters) and also on r_o/r_{in} and t/ℓ.

The two-dimensional efficiency η_{2D} defined as Q_{2D}/Q_{id} is formed by the ratio of equations (12) to (20), and in terms of the dimensionless parameters of appendix D, is given by

$$\eta_{2D} = \frac{-\int_{\varphi=\sin^{-1}(t/\ell)(\ell/r_o)}^{\varphi=(\pi/2)} \frac{\partial\theta}{\partial R} R_o \, d\varphi - \int_{X=\sqrt{R_o^2-L^4}}^{X=R_o+L} \frac{\partial\theta}{\partial Y} dX}{\lambda_{in}\left(1-\theta_s^4\right)(L+R_o)} \tag{21}$$

One-dimensional. - The one-dimensional efficiency, denoted by η_i for method i, is defined as Q_i/Q_{id}. In terms of dimensionless parameters, these ratios become as follows:

$$\eta_1 = \frac{\eta_{in}\frac{\ell}{r_o} + \frac{\pi}{2}}{\frac{\ell}{r_o} + 1} \tag{22}$$

$$\eta_2 = \frac{\eta_{in}\frac{\ell}{r_o} + 1}{\frac{\ell}{r_o} + 1} \tag{23}$$

$$\eta_3 = \frac{\left(\theta_o^4 - \theta_s^4\right)\left(\eta_o\frac{\ell}{r_o} + 1\right)}{\left(1-\theta_s^4\right)\left(\frac{\ell}{r_o} + 1\right)} \tag{24}$$

$$\eta_4 = \frac{0.85\left(\theta_o^4 - \theta_s^4\right)\left(\eta_o \frac{\ell}{r_o} + \frac{\pi}{2}\right)}{\left(1 - \theta_s^4\right)\left(\frac{\ell}{r_o} + 1\right)} \tag{25}$$

$$\eta_5 = \frac{\eta_T\left(\theta_o^4 - \theta_s^4\right)}{1 - \theta_s^4} \tag{26}$$

$$\eta_6 = \frac{\eta_r^{*\bar{\epsilon}}\left(\theta_o^4 - \theta_s^4\right)}{\epsilon\left(1 - \theta_s^4\right)} \tag{27}$$

where

$$\theta_o = \frac{T_o}{T_{in}}$$

RESULTS AND DISCUSSION

Results were obtained for several cases divided into three groups as indicated in table II. Group A consists of several radiators that were designed for various power system applications and are near minimum weight design. These radiators cover a wide range of actual dimensional variables. Group B is a set of parametric cases obtained by choosing three values of each dimensionless variable in order to study the effect on one- and two-dimensional agreement of varying each parameter independently of the others. Group C is a set of off-design Brayton cycle cases. The basic design case is a near-minimum weight radiator for a Brayton cycle space powerplant. This basic design case was altered by arbitrarily varying the inside tube temperature and the outside tube radius.

Radiating Effectiveness

The first results to be presented are the comparison of the one-dimensional radiator effectiveness with the two-dimensional shown in figures 5(a) to (f). The comparison for method 1 is shown in figure 5(a). In all cases the one-dimensional effectiveness is too

TABLE II. - INPUT DATA AND PERCENT DIFFERENCE RESULTS

Case	Material	Physical dimensions								Dimensionless parameters						Percent difference					
		Emittance, ϵ	Temperature, inside tube wall, T_{in}, °R	Inside tube radius, r_{in}, in.	Outside tube radius, r_o, in.	Fin half thickness, t, in.	Fin half length, ℓ, in.	Thermal conductivity, k, Btu/(hr)(ft)(°R)	Equivalent sink temperature, T_s, °R	Conductance parameter λ_{in}	Conductance parameter a_{λ_o}	Fin-tube profile ratio, ℓ/r_o	Radius ratio, r_o/r_{in}	Fin aspect ratio, t/ℓ	Sink temperature ratio, θ_s	E_1	E_2	E_3	E_4	E_5	E_6
Design cases (A)																					
1	Al	0.9	748	0.500	0.695	0.0084	4.17	111	400	1.001	1.00	6.00	1.39	0.00201	0.535	8.6	-4.5	-4.5	-7.7	-2.0	-3.8
2	Al		707	.602	.801	.0129	5.20	110		.864	.864	6.50	1.33	.00248	.566	8.6	-3.4	-3.4	-7.7	-1.3	-3.2
3	Al		838	.095	.293	.0025	1.58	108		.705	.705	5.40	3.07	.00156	.477	8.6	-4.4	-4.4	-7.8	-2.3	-3.7
4	Be		1149	.187	.355	.0078	2.13	75.5		1.50	1.50	6.00	1.89	.00367	.348	11.2	-3.5	-3.7	-5.7	-.3	-2.2
5	Al		1149	.250	.511	.0106	3.07	112		1.54	1.54	6.00	2.04	.00347	.348	11.1	-3.6	-3.8	-5.7	-.4	-2.3
6	SS		1149	.187	.354	.0158	1.06	10		1.39	1.38	3.00	1.89	.0149	.348	19.6	-3.3	-4.7	.1	1.5	.9
7	Al		607	.062	.213	.0034	2.56	110		.503	.502	12.00	3.41	.00133	.659	2.6	-3.6	-3.7	-12.8	-3.3	-5.6
8	Be		1656	.312	.813	.0572	1.63	54		.499	.487	2.00	2.60	.0352	.242	25.4	.7	-2.2	3.5	2.0	2.4
9	Be		1700	.312	.885	.0501	1.74	51.5	0	.740	.719	2.08	2.67	.0288	0	26.0	.4	-3.0	3.5	2.3	2.6
10	Cb		1664	.250	.673	.0402	1.46	34	0	.924	.894	2.17	2.69	.0275	0	26.7	.5	-3.3	3.5	2.7	2.8
11	Al		1125	.086	.320	.0184	2.37	90	700	.623	.622	7.40	3.74	.00774	.622	9.8	-.5	-.7	-7.0	.6	-1.4
12	Cb		2210	.187	.381	.0264	.763	38	0	.804	.781	2.00	2.03	.0346	0	26.4	-.1	-3.4	3.9	2.4	2.7
13	Be		1670	.187	.441	.0258	1.10	49.5	0	.569	.561	2.50	2.35	.0234	0	20.8	-.9	-2.5	1.1	1.4	1.5
Parametric cases (B)																					
1	(b)	(b)	(b)	(b)	(b)	(b)	(b)	(b)	(b)	1.0	0.992	6.0	2.0	0.0250	0.4	15.7	1.8	0.9	-2.6	3.5	1.6
2										.5	.498	6.0				12.7	1.1	.6	-4.7	2.0	.6
3										2.0	1.97	6.0				19.5	2.5	.7	-.3	5.0	3.0
4										1.0	.953	1.0				33.8	-2.5	-8.4	7.0	-.1	1.7
5											.997	15.0				9.5	3.0	2.6	-7.2	3.2	0
6											.996	6.0	1.4			13.7	.1	-.4	-3.8	2.2	-.4
7											.987		3.0			17.4	3.4	1.9	-1.7	4.5	2.6
8											.984		2.0	.05		20.0	5.6	3.7	.1	6.4	4.5
9											.994			.0167		13.9	.3	-.4	-3.8	2.3	.4
10											.995			.025	.8	16.3	2.0	1.0	-2.1	3.9	1.8
11											.991			.025	0	15.6	1.8	.9	-2.7	3.5	1.6
Off-design Brayton cases (C)																					
1	Be	0.9	884	0.5	1.2	0.0770	7.21	60	400	0.999	0.994	6.0	2.4	0.0107	0.452	12.8	-0.7	-1.2	-4.6	1.4	-0.5
2					.6						.998	12.0	1.2			6.9	-.8	-.8	-9.2	.1	-2.7
3					1.8						.989	4.0	3.6			16.5	-1.4	-2.5	-2.1	1.4	.3
4					.9						.997	8.0	1.8			10.4	-.4	-.7	-6.4	1.1	-1.3
5					1.5						.992	4.8	3.0			14.8	-1.1	-1.9	-3.2	1.5	0
6			536		1.2					.223	.223	6.0	2.4		.746	9.2	-.7	-.8	-7.3	-.6	-1.3
7			756							.625	.623				.529	11.4	-.6	-1.0	-5.6	.8	-.8
8			976							1.34	1.34				.410	13.8	-.8	-1.5	-3.9	1.7	-.2
9			1196							2.47	2.45				.334	16.2	-1.2	-2.3	-2.4	2.5	.5
10			1400							3.97	3.90				.286	18.5	-1.4	-3.3	-1.2	3.1	1.2
11			1550							5.38	5.25				.258	20.3	-1.5	-4.0	-.5	3.5	1.7
12			1700							7.10	6.88				.235	22.1	-1.5	-4.7	.1	3.8	2.2
13			1850							9.16	8.79				.216	24.0	-1.3	-5.5	.7	4.1	2.6
14			2000							11.57	10.99				.200	26.0	-.9	-6.2	1.1	4.4	3.0
15			2130							13.97	13.15				.188	27.9	-.4	-6.8	1.4	4.7	3.4

[a] a_{λ_o} is not an independent parameter in the two-dimensional method but is in some of the one-dimensional methods.

[b] Physical dimensions not applicable.

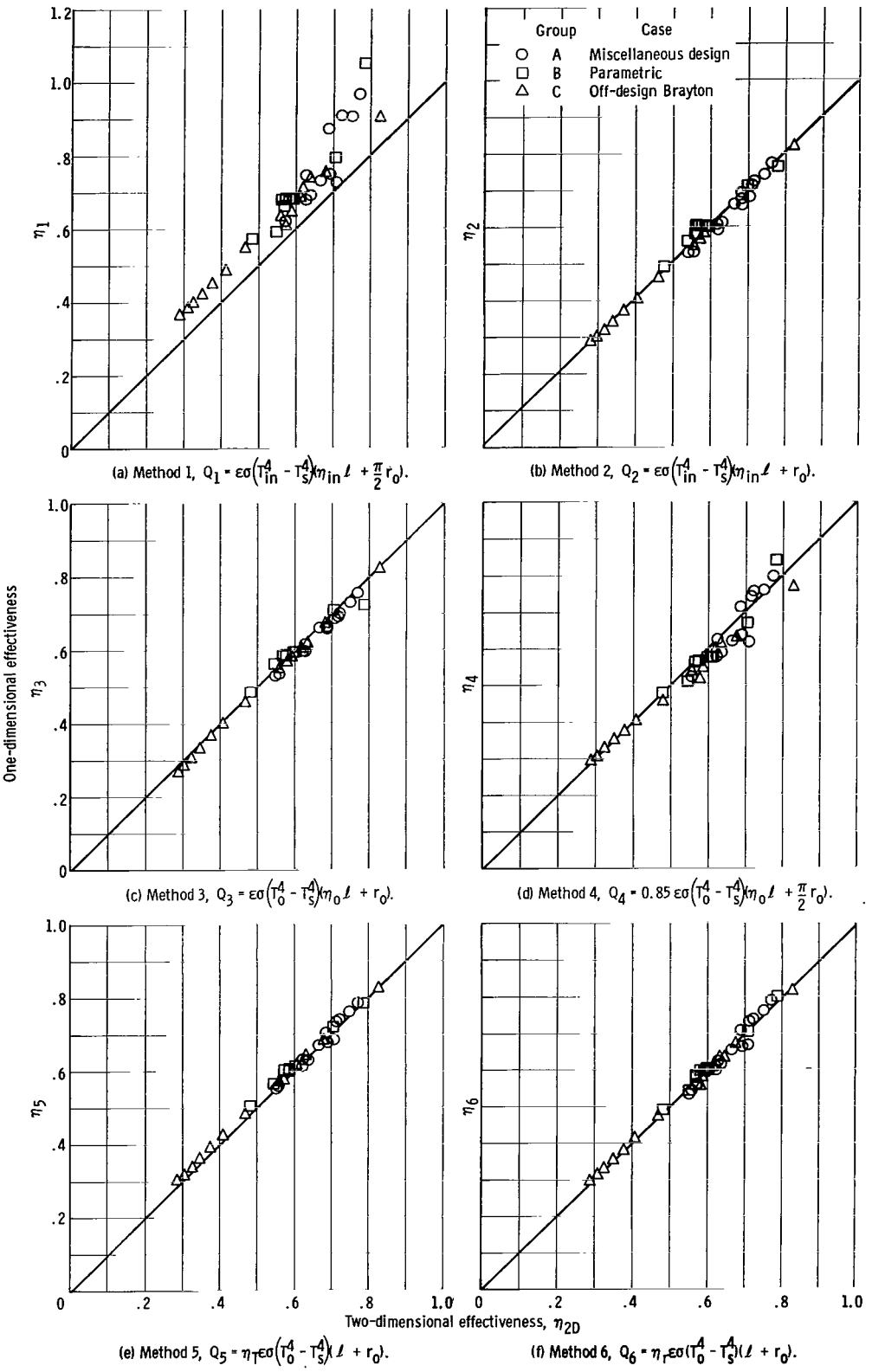

Figure 5. - Comparison of overall effectiveness obtained by one-dimensional methods with that obtained by two-dimensional method.

large, all the points falling above the line of equality. This is because method 1 neglects the temperature drop in the tube and uses the actual tube area without allowing for any interchange with the result that the calculated tube heat rejection rate is too high. Thus the worst points on figure 5(a) are for cases having a relatively small value of ℓ/r_o (as can be seen in table II), which makes the tube heat rejection contribution more important.

Figure 5(b) shows the comparison for method 2. Here the agreement is quite good even though the temperature drop in the tube is neglected.

The comparison for method 3 is shown in figure 5(c). Here the agreement is also quite good but no better than for method 2. Method 3 is the same as method 2 except that the temperature drop in the tube is taken into account. Thus, for the range of cases studied, the tube wall temperature drop seems relatively unimportant.

The comparison for method 4 is shown in figure 5(d). The agreement is fair but there is considerable scatter. This is probably due to the attempt to account for the radiant interchange by using the constant factor of 0.85.

Figure 5(e) shows the comparison for method 5. Here the agreement is quite good and there is very little scatter. It is no better, however, than methods 2 or 3 which are simpler. There is also quite good agreement and very little scatter in figure 5(f), which shows the comparison for method 6. Method 6 is not significantly better than methods 2 or 3 but it is the most complicated of all the one-dimensional methods.

To summarize, one-dimensional methods 2, 3, 5, and 6 show good agreement with two-dimensional; whereas method 1 shows very poor agreement and method 4 shows fair agreement.

Percent Difference

The agreement between one- and two-dimensional calculation can also be evaluated by the percent difference E_i defined as

$$E_i = 100\left(\frac{Q_i}{Q_{2D}} - 1\right) = 100\left(\frac{\eta_i}{\eta_{2D}} - 1\right) \tag{28}$$

The percent difference for each method and for each case analyzed is given in table II. Here the agreement can be seen in relation to the input parameters of the various groups of cases. It should be noted that a positive percent difference means that the one-dimensional method is predicting too high a heat rejection rate, and a negative percent difference means too low a rate.

The percent difference data is summarized in table III in the form of average abso-

TABLE III. - SUMMARY OF DIFFERENCE DATA

Group	Number of cases	Method					
		1	2	3	4	5	6
Average absolute percent difference							
A	13	15.8	2.3	3.3	5.4	1.7	2.7
B	11	17.1	2.2	1.9	3.3	3.3	1.7
C	15	16.7	1.0	2.9	3.3	2.3	1.4
Overall (A, B, and C)	39	16.5	1.8	2.8	4.0	2.4	1.9
Maximum absolute percent difference							
A	13	26.5	4.5	4.7	12.8	3.3	5.6
B	11	33.8	5.6	8.4	7.0	6.4	4.5
C	15	27.9	1.5	6.8	9.2	4.7	3.4

lute values of percent difference and the maximum absolute value of percent difference. As in figure 5, it can be seen here that methods 2, 3, 5, and 6 are in good agreement with the two-dimensional method. The best methods, on the average, are 2 and 6, with values of average absolute percent difference of 1.8 and 1.9, respectively. Both methods have a value of 5.6 for the maximum absolute percent difference, which is an indication of the performance of a method at its worst. Thus it appears that for the average radiator configurations likely to be encountered, method 2 will give as close agreement with the two-dimensional as method 6. Method 2 has the advantage of being simpler than method 6.

The heat rejection formula for method 2 (eq. (14)) contains only prescribed quantities except for η_{in} which is a function of λ_{in} and T_s/T_{in}. Curves for η_{in} are readily available in the literature (e.g., ref. 9). Furthermore, T_s/T_{in} can often be assumed to be zero and only one curve (η_{in} against λ_{in}) need be used. On the other hand, the formula for method 6 (eq. (18)), contains three quantities not directly prescribed T_o, η_r^*, and $\bar{\epsilon}$. The outside tube wall temperature T_o is calculated by assuming one-dimensional radial heat conduction in a radiating tube. The overall blackbody effectiveness η_r^* is a function of N_c, ℓ/r_o, and T_s/T_o; T_s/T_o is often assumed to be zero and η_r^* is obtained by interpolation from plots of η_r^* against ℓ/r_o and N_c (ref. 5). The apparent emissivity $\bar{\epsilon}$ is a function of ϵ, ℓ/r_o, and T_s/T_o; here T_s/T_o is assumed to be zero and $\bar{\epsilon}$ is obtained by interpolation from plots of $\bar{\epsilon}$ against ℓ/r_o and ϵ (ref. 5).

Because of its simplicity and accuracy, method 2 is recommended for central fin-tube radiator calculations except for cases with very large r_o/r_i (say, greater than 4.0). For these latter cases, method 3, which is only slightly more complicated (the temperature drop in the tube must be calculated), can be used.

Effect of Input Parameters on Percent Difference

The cases of group B in table II were analyzed in order to determine the effect of the independent dimensionless parameters on percent difference. Case B1 is the standard case and its parameters have typical values as obtained in current near-minimum-weight

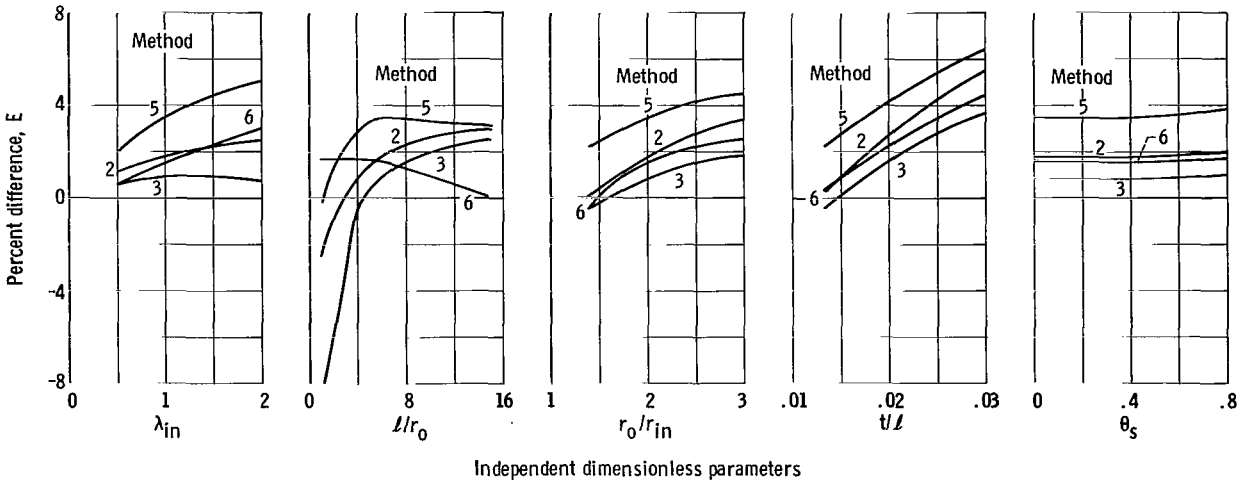

Figure 6. - Effect of change in independent dimensionless parameters on percent difference.

design studies at Lewis. The other cases were obtained by holding all parameters but one constant and taking high and low extreme values spanning the range of current interest. For example, case B1 has a λ_{in} of 1.0, case B2 of 0.5, and case B3 of 2.0 with the other parameters being identical for all three cases. This results in three data points for each parameter. The results are shown in figure 6 for one-dimensional methods 2, 3, 5, and 6. It should be pointed out that the level of the curves (i.e., their location relative to zero percent difference) is the result of the particular set of parameters chosen for the standard case.

In looking at all the parts of figure 6, it can be seen that, in general, variation in ℓ/r_o has the greatest effect (particularly at small ℓ/r_o), variation in t/ℓ has the next greatest effect, and variation in θ_s has practically no effect. Another general observation is that all four methods exhibit essentially the same trends except for the ℓ/r_o curve for method 6.

CONCLUSIONS

Results of the two-dimensional analysis of the heat transfer in the cross section of a central fin-tube radiator have been used to evaluate several one-dimensional methods of calculating the heat rejection rate of such radiators. Most of the one-dimensional methods give good agreement with the two-dimensional; however, they are of varying degrees of complexity. In view of the good agreement of the method (number 2) that neglects tube

wall temperature drop and accounts for radiant interchange simply by using the projected area of the tube, it seems unwarranted to use more complicated methods.

Lewis Research Center,
National Aeronautics and Space Administration,
Cleveland, Ohio, June 30, 1966,
120-27-04-36-22.

APPENDIX A

SYMBOLS

A	area of radiator surface per unit axial length
B	radiosity, sum of emitted plus reflected energy leaving surface per unit time and area
$\mathscr{B}$	$B/\sigma T_{in}^4$
dA^*	particular element of area
E_i	percent difference of method i
F_{1-2}	view factor, fraction of radiant energy leaving surface 1 that strikes surface 2
H	total energy incident on a surface per unit time and unit area
$\mathscr{H}$	$H/\sigma T_{in}^4$
k	thermal conductivity, summation index (appendix C)
L	$\ell t/\ell^2 = t/\ell$
ℓ	fin half length, see fig. 2
N_c	blackbody conductance parameter, $\sigma T_o^3 \ell^2/kt$
Q	calculated heat rejection rate
Q_{id}	ideal heat rejection rate, eq. (20)
q	energy radiated per unit time and per unit area
R	rt/ℓ^2
r	radial coordinate in tube
S	arbitrary surface representing surroundings
T	temperature
T_s	equivalent sink temperature
t	fin half thickness, see fig. 2
X	xt/ℓ^2
x	horizontal coordinate in fin
Y	yt/ℓ^2
y	vertical coordinate in fin
α	absorptance
ϵ	emittance
$\bar{\epsilon}$	apparent emissivity
η	overall efficiency
η_{in}	fin efficiency based on T_{in}
η_o	fin efficiency based on T_o
η_r^*	overall effectiveness, ref. 5
η_T	overall effectiveness, refs. 4 and 6
θ	dimensionless temperature, T/T_{in}
λ	conductance parameter, $\epsilon\sigma T_b^3 \ell^2/kt$
ρ	reflectance
σ	Stefan-Boltzmann constant
φ	angular coordinate in tube, see fig. 3
ω	overrelaxation parameter, appendix C

Subscripts:

b	fin base
2D	based on two-dimensional analysis
i	based on one-dimensional method i, i = 1, 2 . . . 6

i, j, k	indices, appendix C
in	inside tube wall
L	lower limit of visibility
o	outside tube wall
S	referring to area of arbitrary surface S
U	upper limit of visibility
1	tube 1
2	tube 2

Superscript:

m	iteration number, appendix C

APPENDIX B

DERIVATION OF EQUATION FOR INCIDENT RADIATION

The total radiation H_{dA^*} incident on an element dA^* of the fin or tube is made up of radiation from other parts of the fin or tube and radiation from the surroundings. In equation form,

$$H_{dA^*} = q_{A-dA^*} + q_{S-dA^*} \tag{B1}$$

where q_{A-dA^*} is the heat per unit time leaving all of the fin and tube surface A and striking a unit area of dA^*, and q_{S-dA^*} is the heat per unit time leaving the surroundings or sink which may be represented by an arbitrary surface S (fig. 7) and striking a unit area of dA^*. The q's are given by

$$q_{A-dA^*} = \frac{Q_{A-dA^*}}{dA^*} \tag{B2}$$

and

$$q_{S-dA^*} = \frac{Q_{S-dA^*}}{dA^*} \tag{B3}$$

where Q_{A-dA^*} is the heat per unit time leaving all of A and striking all of dA^*, and Q_{S-dA^*} is that leaving all of S and striking all of dA^*. The Q's are given by

$$Q_{A-dA^*} = \int_A B_{dA}\, dA\, dF_{dA-dA^*} \tag{B4}$$

and

$$Q_{S-dA} = \sigma T_s^4 S\, dF_{S-dA^*} \tag{B5}$$

where B_{dA} is the radiosity, that is, the total energy emitted plus reflected leaving dA per unit time, dF_{dA-dA^*} is the view factor from dA to dA^*, T_s is the equivalent sink temperature of the surroundings, S is the area of surface S, and dF_{S-dA^*} is the view

factor from S to dA*. From the reciprocity theorem for view factors,

$$dA\, dF_{dA-dA^*} = dA^*\, dF_{dA^*-dA} \tag{B6}$$

and

$$S\, dF_{S-dA^*} = dA^* F_{dA^*-S} \tag{B7}$$

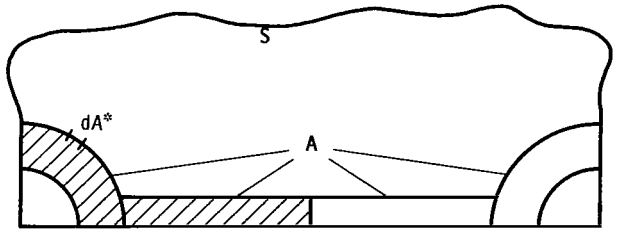

Figure 7. - Surfaces involved in incident radiation.

Furthermore, all the energy leaving dA* strikes either part of S or part of A (see fig. 7) so that

$$F_{dA^*-S} = 1 - \int_A dF_{dA^*-dA} \tag{B8}$$

Combining equations (B6), (B4), and (B2) yields

$$q_{A-dA^*} = \int_A B_{dA}\, dF_{dA^*-dA} \tag{B9}$$

Combining equations (B8), (B7), (B5), and (B3), yields

$$q_{S-dA^*} = \sigma T_s^4 \left(1 - \int_A dF_{dA^*-dA}\right) \tag{B10}$$

Putting equations (B9) and (B10) into equation (B1) yields the expression for the total energy incident on dA* per unit time:

$$H_{dA^*} = \int_A B_{dA}\, dF_{dA^*-dA} + \sigma T_s^4 \left(1 - \int_A dF_{dA^*-dA}\right) \tag{8}$$

APPENDIX C

NUMERICAL METHOD OF SOLUTION

The nonlinearity of the boundary conditions and the geometry preclude the possibility of a closed form solution of the problem outlined in the Equations and Boundary Conditions section (p. 4). Hence, it was necessary to attack the problem numerically. The numerical solution was obtained by replacing equations (2), (3), and (10) by their finite-difference analogues at points of a grid as shown in figure 3 (p. 4). The solution of the partial differential equations satisfies these difference equations except for an error term which vanishes when the grid spacing approaches zero. This in turn is reflected in an error in the temperatures at the grid points which likewise vanishes as the grid is refined.

The set of points at which the temperatures are obtained consists of the points of intersection of the polar grid lines in the tube and the points of intersection of the rectangular grid lines in the fin (fig. 3). The spacings of the rays and circular arcs in the tube and verticals in the fin are prescribed. The arcs in the tube and the verticals in the fin are uniformly spaced. For the spacing of rays in the tube, however, the tube is divided into two regions of uniform ray spacings; the ray spacings near the fin are finer than the spacings away from the fin (as illustrated in fig. 3) since the temperature gradients are more severe near the fin. The spacing of the horizontals in the fin is determined by the ends of the rays in the tube at the intersection of the tubes and fin and is thus not uniform. After this main grid is specified, a dual grid is constructed by bisecting the lines of the grid just described. This results in a closed cell about each point of the original grid. The boundaries of the cells are the dashed lines shown in figure 8.

The finite-difference equations for the temperatures are obtained by integrating Laplace's equation over cells of the dual grid, replacing the normal derivatives arising from the use of the divergence theorem by difference quotients exactly as on pages 17 and 18 of reference 11. In the present case, however, the cells of the dual grid are not all rectangles as they are in reference 11, but some are annular sectors in the tube and some are irregularly shaped cells in the transition region, one of which is shaded in figure 8. The result is that the difference equations in the tube have coefficients modified by lengths of arcs and chords and those in the transition region entail six points instead of five.

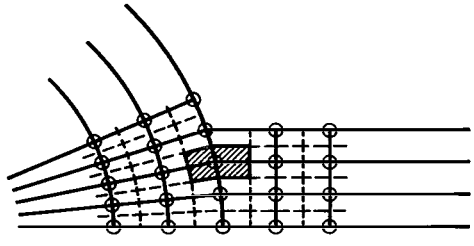

Figure 8. - Cell for integration around point on intersection of fin and tube.

The finite-difference equations for the radiosities are obtained by substituting a simple quadrature formula for the integral in equation (10), so that it reads

$$B_{dA_j} = \epsilon \sigma T_{dA_j}^4 + (1 - \epsilon) \left[\sum_k B_{dA_k} \, dF_{dA_j - dA_k} + \sigma T_s^4 \left(1 - \sum_k dF_{dA_j - dA_k} \right) \right] \tag{C1}$$

where the summation is carried out over those elements dA_k that are visible from element dA_j.

The result of the discretization is two sets of difference equations: one set is derived from equations (2) and (3) at interior points and from equations (2) to (7b) at boundary points, and a second set is derived from equation (10). The first set is a system of equations for the temperature interior to and on the surface of the tube and fin with the values of radiosities as input to the equations at the surface points. These latter equations were linearized by replacing T^4 by $\left[T^{(m-1)}\right]^4 + 4\left[T^{(m-1)}\right]^3 \left[T - T^{(m-1)}\right]$ wherever it appears. Here the superscripts refer to iteration number, and $m = 1$ corresponds to the initial approximation. The second set, typified by equation (C1) is a system of linear equations for the radiosities with the values of surface temperatures as input. Initially, very coarse approximations were made to both temperature and radiosity. Then one iteration of the block successive over relaxation method was carried out on the first set of equations. This single iteration for the temperatures was followed by as many iterations as needed for convergence of the Gauss-Seidel method on the linear system of equations for the radiosities (very few iterations were needed for this step). This process was repeated, alternating between the two sets of equations until convergence was obtained. It was found that comparison of the net heat radiated by the fin and tube surfaces with that flowing into the inside surface of the tube supplied a practical criterion for the convergence of the iterative process.

The block successive overrelaxation method mentioned previously was like that described on pages 19 and 20 of reference 11, at least in the fin. In the tube, the iteration proceeded along similar lines except that here temperatures along a given ray were solved for simultaneously. The iteration started with the vertical ray (at $\varphi = \pi/2$), proceeded to each ray in turn until the horizontal ray ($\varphi = 0$) was reached. Then the iteration proceeded to the verticals from left to right in the fin.

In the iterative method mentioned previously, there is an overrelaxation parameter ω, which is free to be chosen subject to the restriction $0 < \omega < 2$. It has been shown (ref. 12, ch. 4) for systems of linear equations that there is an optimum value of ω for which convergence is fastest. Due to the nonlinearity of the problem involved herein, no rigorous analysis exists for the determination of a corresponding optimum value for ω. Numerical experiments carried out at the Lewis Research Center, however, indicated the validity of the concept of an optimum value, and values of ω obtained in these experi-

ments were used for the production runs. A typical result is $\omega = 1.93$ for 690 points leading to convergence of the relative error in the heat balance to less than 1.0 percent in 180 iterations.

APPENDIX D

NONDIMENSIONAL PARAMETERS AND EQUATIONS

In order to facilitate comparison of the two-dimensional results with one-dimensional results, several dimensionless quantities are formed. This set of parameters results from forcing the conventional one-dimensional conductance parameter λ_{in} to appear:

$$\left.\begin{aligned} \theta &\equiv \frac{T}{T_{in}} & R &\equiv \frac{rt}{\ell^2} \\ \theta_s &\equiv \frac{T_s}{T_{in}} & \lambda_{in} &\equiv \frac{\epsilon\sigma T_{in}^3 \ell^2}{kt} \\ X &\equiv \frac{xt}{\ell^2} & \mathscr{B} &\equiv \frac{B}{\sigma T_{in}^4} \\ Y &\equiv \frac{yt}{\ell^2} & \mathscr{H} &\equiv \frac{H}{\sigma T_{in}^4} \end{aligned}\right\} \qquad \text{(D1)}$$

Putting these parameters into the dimensional equations and boundary conditions results in the following:

In the tube:

$$\frac{1}{R}\frac{\partial\theta}{\partial R} + \frac{\partial^2\theta}{\partial R^2} + \frac{1}{R^2}\frac{\partial^2\theta}{\partial\varphi^2} = 0 \qquad \text{(D2)}$$

In the fin:

$$\frac{\partial^2\theta}{\partial X^2} + \frac{\partial^2\theta}{\partial Y^2} = 0 \qquad \text{(D3)}$$

Along the inside tube wall where $R = R_{in} = r_{in}t/\ell^2 = (r_{in}/\ell)(t/\ell)$:

$$\theta(R_{in}, \varphi) = 1.0 \tag{D4}$$

Along $\varphi = 0$ and $\varphi = \pi/2$ in the tube:

$$\left(\frac{\partial\theta}{\partial\varphi}\right)_{\varphi=0} = \left(\frac{\partial\theta}{\partial\varphi}\right)_{\varphi=(\pi/2)} = 0 \tag{D5}$$

Along $Y = 0$ and $X = (\ell + r_o)t/\ell^2 = (1 + r_o/\ell)t/\ell$:

$$\left(\frac{\partial\theta}{\partial Y}\right)_{Y=0} = \left(\frac{\partial\theta}{\partial X}\right)_{X=(1+r_o/\ell)t/\ell} = 0 \tag{D6}$$

On the surface of the tube where $R = R_o = r_o t/\ell^2 = (r_o/\ell)(t/\ell)$:

$$-\left(\frac{\partial\theta}{\partial R}\right)_{R=R_o} = \lambda_{in}(\theta^4 - \mathscr{H}) \tag{D7a}$$

On the surface of the fin where $Y = t^2/\ell^2$:

$$-\left(\frac{\partial\theta}{\partial Y}\right)_{Y=t^2/\ell^2} = \lambda_{in}(\theta^4 - \mathscr{H}) \tag{D7b}$$

where

$$\mathscr{H}_{dA^*} = \theta_s^4\left(1 - \int_A dF_{dA^*\text{-}dA}\right) + \int_A \mathscr{B}_{dA}\, dF_{dA^*\text{-}dA} \tag{D8}$$

and

$$\mathscr{B}_{dA^*} = \epsilon\theta_{dA^*}^4 + (1 - \epsilon)\left[\int_A \mathscr{B}_{dA} dF_{dA^*\text{-}dA} + \theta_s^4\left(1 - \int_A dF_{dA^*\text{-}dA}\right)\right] \tag{D9}$$

Thus, it can be seen that the dimensionless temperature θ depends on the parameters λ_{in}, r_{in}/ℓ, r_o/ℓ, t/ℓ, θ_s, and ϵ. In this report, ϵ will always be fixed at 0.9 and can

be eliminated from the list of variables. Of the remaining parameters, λ_{in}, r_o/ℓ (often written ℓ/r_o), and θ_s are the commonly used one-dimensional parameters and r_{in}/ℓ and t/ℓ are two-dimensional parameters. Instead of r_{in}/ℓ, it is more informative to use r_o/r_{in}, which is the ratio of r_o/ℓ to r_{in}/ℓ. To summarize, in this report the parameters determining the two-dimensional heat transfer in a fin-tube radiator are λ_{in}, r_o/ℓ (or ℓ/r_o), θ_s, r_o/r_{in}, and t/ℓ.

REFERENCES

1. Schreiber, L. H.; Mitchell, R. P.; Gillespie, G. D.; and Olcott, R. M.: Techniques for Optimization of a Finned-Tube Radiator. Paper No. 61-SA-44, ASME, June 1961.

2. Callinan, Joseph P.; and Berggren, Willard P.: Some Radiator Design Criteria for Space Vehicles. J. Heat Transfer, vol. 81, no. 3, Aug. 1959, pp. 237-244.

3. Mackay, D. B.; and Bacha, C. P.: Space Radiator Analysis and Design. Part I. Rep. No. SID 61-66 (AFASD TR 61-30, pt. 1), North American Aviation, Inc., Apr. 1, 1961, pp. 11-22.

4. Haller, Henry C.; Wesling, Gordon C.; and Lieblein, Seymour: Heat-Rejection and Weight Characteristics of Fin-Tube Space Radiators with Tapered Fins. NASA TN D-2168, 1964.

5. Krebs, Richard P.; Haller, Henry C.; and Auer, Bruce M.: Analysis and Design Procedures for a Flat, Direct-Condensing, Central Finned-Tube Radiator. NASA TN D-2474, 1964.

6. Saule, Arthur V.; Krebs, Richard P.; and Auer, Bruce M.: Design Analysis and General Characteristics of Flat-Plate Central-Fin-Tube Sensible-Heat Space Radiators. NASA TN D-2839, 1965.

7. Sparrow, E. M.; and Eckert, E. R. G.: Radiant Interaction Between Fin and Base Surfaces. J. Heat Transfer, vol. 84, no. 1, Feb. 1962, pp. 12-18.

8. Krebs, Richard P.; Winch, David M.; and Lieblein, Seymour: Analysis of a Megawatt Level Direct Condenser-Radiator. Power Systems for Space Flight. Vol. 11 of Progress in Astronautics and Aeronautics, Morris Zipkin and Russell N. Edwards, eds., Academic Press, Inc., 1963, pp. 475-504.

9. Lieblein, Seymour: Analysis of Temperature Distribution and Radiant Heat Transfer Along a Rectangular Fin of Constant Thickness. NASA TN D-196, 1959.

10. Sotos, Carol J.; and Stockman, Norbert O.: Radiant-Interchange View Factors and Limits of Visibility for Differential Cylindrical Surfaces with Parallel Generating Lines. NASA TN D-2556, 1964.

11. Stockman, Norbert O.; and Bittner, Edward C.: Two-Dimensional Heat Transfer in Radiating Stainless-Steel-Clad Copper Fins. NASA TN D-3102, 1965.

12. Varga, R. S.: Matrix Iterative Analysis. Prentice-Hall, Inc., 1962.

"The aeronautical and space activities of the United States shall be conducted so as to contribute . . . to the expansion of human knowledge of phenomena in the atmosphere and space. The Administration shall provide for the widest practicable and appropriate dissemination of information concerning its activities and the results thereof."

—NATIONAL AERONAUTICS AND SPACE ACT OF 1958

NASA SCIENTIFIC AND TECHNICAL PUBLICATIONS

TECHNICAL REPORTS: Scientific and technical information considered important, complete, and a lasting contribution to existing knowledge.

TECHNICAL NOTES: Information less broad in scope but nevertheless of importance as a contribution to existing knowledge.

TECHNICAL MEMORANDUMS: Information receiving limited distribution because of preliminary data, security classification, or other reasons.

CONTRACTOR REPORTS: Technical information generated in connection with a NASA contract or grant and released under NASA auspices.

TECHNICAL TRANSLATIONS: Information published in a foreign language considered to merit NASA distribution in English.

TECHNICAL REPRINTS: Information derived from NASA activities and initially published in the form of journal articles.

SPECIAL PUBLICATIONS: Information derived from or of value to NASA activities but not necessarily reporting the results of individual NASA-programmed scientific efforts. Publications include conference proceedings, monographs, data compilations, handbooks, sourcebooks, and special bibliographies.

Details on the availability of these publications may be obtained from:

SCIENTIFIC AND TECHNICAL INFORMATION DIVISION

NATIONAL AERONAUTICS AND SPACE ADMINISTRATION

Washington, D.C. 20546